ChemComm

COMMUNICATION

View Article Online
View Journal | View Issue

Cite this: *Chem. Commun.*, 2016, 52, 13373

Received 20th September 2016,
Accepted 21st October 2016

DOI: 10.1039/c6cc07645a

www.rsc.org/chemcomm

Synchronous exfoliation and assembly of graphene on 3D $Ni(OH)_2$ for supercapacitors†

Liguo Ma,[a] Maojun Zheng,*[ab] Shaohua Liu,*[c] Qiang Li,[a] Yuxiu You,[a] Faze Wang,[a] Li Ma[d] and Wenzhong Shen[a]

Nowadays, new approaches to fabricate high-performance electrode materials are of vital importance in the renewable energy field. Here, we present a facile synthesis procedure of 3D $Ni(OH)_2$/graphene hybrids for supercapacitors *via* synchronous electrochemical-assisted exfoliation and assembly of graphene on 3D $Ni(OH)_2$ networks. With the assistance of an electric field, the electrochemically exfoliated high-quality graphene can be readily, uniformly assembled on the surfaces of 3D $Ni(OH)_2$. When serving as electrode materials for supercapacitors, the resulting 3D $Ni(OH)_2$/graphene composites exhibited excellent specific capacitance (263 mF cm^{-2} at 2 mA cm^{-2}), remarkable rate capability and super-long cycle life (retention of 94.1% even after 10 000 continuous charge–discharge cycles), which may be attributed to their highly porous, stable 3D architecture as well as uniform, firm anchoring of ultrathin graphene on their surfaces. Therefore, our approach provides a facile strategy for the large-scale synthesis of high-quality graphene based composites towards various applications.

Supercapacitors with high capacitance and long lifespan have attracted considerable interest as energy-storage devices in recent years. At present, two kinds of supercapacitors have been developed based on the charge storage mechanism: electric double-layer capacitors and pseudocapacitors. By comparison, pseudocapacitors governed by Faradaic reactions at the electrode materials, such as RuO_2,[1] MnO_2,[2] NiO,[3] Co_3O_4,[4] and CuO,[5] have higher theoretical capacitance. Despite that, those electrode materials usually suffer from poor stability, low conductivity and large volume change during charge/discharge processes.[6] Among the various redox-active materials, $Ni(OH)_2$ is an attractive candidate for high-performance supercapacitors because of its low-cost, various morphologies, high theoretical capacitance, ready availability and good stability in alkaline electrolytes.[7] In attempts to further improve the electrochemical performance of $Ni(OH)_2$-based electrodes, $Ni(OH)_2$/carbon composites involving high surface-area conductive materials (carbon nanotubes,[8] activated carbon[9] and graphene[10]) have been explored. However, the fabrication of $Ni(OH)_2$/carbon electrodes usually needs multi-step procedures. Taking $Ni(OH)_2$/graphene as an example, graphene needs to be firstly prepared by Hummer's method or modified Hummer's method, and subsequently grows on $Ni(OH)_2$ surfaces by hydrothermal treatment.[11] Obviously, such fabrication processes are complicated and costly for supercapacitor applications.

Recently, high-quality graphene can be produced by a simple, fast and green electrochemical exfoliation method. Müllen *et al.*[12] manufactured high-quality few-layer graphene through anodic exfoliation. Yan *et al.*[13] used a Na_2SO_4-containing electrolyte and other metal sulfate salts to exfoliate graphite and further fabricate Fe_2O_3–, Co_3O_4– and V_2O_5–graphene hybrids. Ji *et al.*[14] produced NiO quantum dots/graphene flakes for supercapacitor applications by a green, one-step alternating voltage method. Nevertheless, one-step fabrication of $Ni(OH)_2$/graphene hybrid materials by synchronous electrochemical-assisted exfoliation and assembly for supercapacitor electrodes still remains unrealized so far.

Here, for the first time, we demonstrate a facile approach for the preparation of $Ni(OH)_2$/graphene composites *via in situ* assembly of exfoliated graphene on 3D $Ni(OH)_2$ surfaces. As illustrated in Fig. 1, ultrathin high-quality graphene was obtained by the solution-based electrochemical exfoliation with a two-electrode system, using graphite flakes, Ni foam and a mixed solution containing $NH_3{\cdot}H_2O$ and $(NH_4)_2SO_4$ (Fig. 1a) as the anode, cathode and electrolyte, respectively. When a direct current voltage of 8 V was applied to a two-electrode setup, vigorous bubbles were produced at electrodes, anodic graphite began to dissociate to form graphene sheets, suspended in the

[a] *Key Laboratory of Artificial Structure and Quantum Control, Ministry of Education, Department of Physics and Astronomy, Shanghai Jiao Tong University, Shanghai, 200240, P. R. China. E-mail: mjzheng@sjtu.edu.cn; Fax: +86-021-54741040*
[b] *Collaborative Innovation Center of Advanced Microstructures, Nanjing University, Nanjing, 210093, P. R. China*
[c] *Center for Advancing Electronics Dresden (cfaed) & Department of Chemistry and Food Chemistry, Dresden, 01062, Germany. E-mail: shaohua.liu@tu-dresden.de*
[d] *School of Chemistry and Chemical Technology, Shanghai Jiao Tong University, Shanghai, 200240, P. R. China*

† Electronic supplementary information (ESI) available. See DOI: 10.1039/c6cc07645a

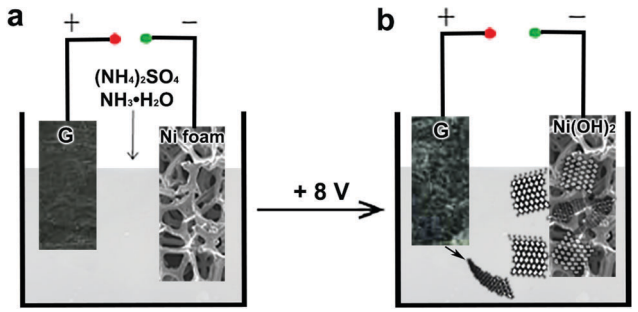

Fig. 1 Schematic illustration of one-step fabrication of $Ni(OH)_2$/graphene composites. (a) Setup of the electrochemical exfoliation of graphite (G). (b) The electrochemical exfoliation process of the graphite electrode and synchronous assembly of graphene on 3D $Ni(OH)_2$.

electrolyte (Fig. 1b). Meanwhile, the cathodic Ni foam firstly transformed into $Ni(OH)_2$ through $NH_3{\cdot}H_2O$ treatment following reactions (1) and (2):

$$Ni + 6NH_3 + 2H_2O \rightarrow [Ni(NH_3)_6]^{2+} + 2OH^- + H_2\uparrow \quad (1)$$

$$Ni^{2+} + 2OH^- \rightarrow Ni(OH)_2 \quad (2)$$

The morphology and structure of the exfoliated graphene sheets were investigated by SEM, TEM and Raman spectroscopy shown in Fig. S1–S3 (ESI†), which clearly demonstrate the formation of high-quality few-layer graphene.[12] Further, graphene obtained by electrochemical-assisted exfoliation would spontaneously absorb and assemble on the cathodic 3D $Ni(OH)_2$ due to electrostatic interaction. Despite high quality, the resulting graphene derived from electrochemical-assisted exfoliation still possesses a few negative charges around its edges,[12] which would prompt their assembly on the $Ni(OH)_2$ surfaces with the assistance of an electric field. Notably, the Ni foam is not only the nickel source for the growth of $Ni(OH)_2$ thin layers, but also a skeleton to support the active materials of $Ni(OH)_2$/graphene composites, which affords a good electrical contact and strong mechanical adherence to their interfaces.[15]

The structure of the $Ni(OH)_2$/graphene composites was further characterized by Raman spectroscopy (Fig. 2a). The Raman spectrum of the $Ni(OH)_2$/graphene composites presents three obvious characteristic vibration bands at 1350 cm^{-1}, 1583 cm^{-1} and 2700 cm^{-1} corresponding to the D, G and 2D band of graphene, respectively. In addition, the $Ni(OH)_2$/graphene composites also present four peaks from $Ni(OH)_2$, at around 315 and 450 cm^{-1} (longitudinal optical, $A_{1g}(T)$ and $E_g(T)$), 983.5 cm^{-1} (phonon mode, $E_g(R)$) and 3580 cm^{-1} (internal hydroxyl symmetric stretching mode, $A_{1g}(I)$).[16]

X-ray photoelectron spectroscopy (XPS) was used to estimate various chemical states of bonded elements. Typical spectra of the as-prepared 3D $Ni(OH)_2$/graphene samples are presented in Fig. 2b–d. A single peak at around 840.8 eV presents the Ni LMM Auger spectrum.[17] The Ni 2p XPS spectrum shows two major peaks centered at around 874.9 eV and 857.3 eV, corresponding to Ni $2p_{1/2}$ and Ni $2p_{3/2}$, respectively. The characteristic of the $Ni(OH)_2$ phase with a spin-energy separation of 17.6 eV coincides with a previous report.[18] Moreover, a strong peak of the

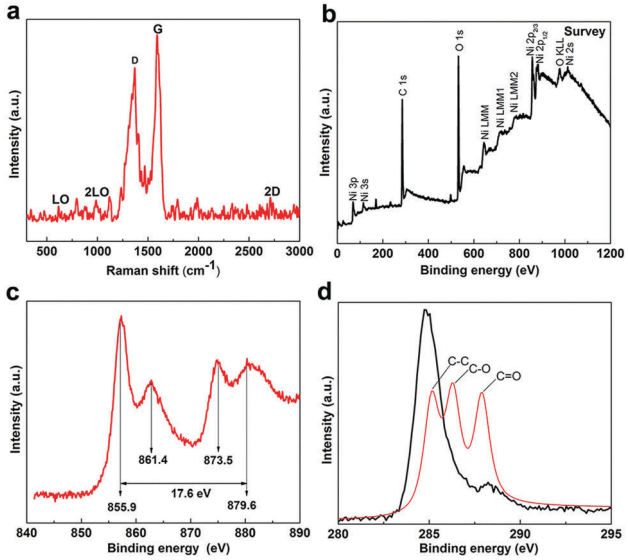

Fig. 2 (a) Raman pattern (excitation laser wavelength: 532 nm) and (b–d) XPS spectra of the $Ni(OH)_2$/graphene samples.

O 1s spectrum at 532.3 eV is also associated with hydroxide groups (OH^-), suggestive of the presence of $Ni(OH)_2$.[18] Additionally, the XPS spectrum of C 1s shows three signals of C–C (284.6 eV), C–O (286.7 eV) and O–C═O (288.6 eV), which are possibly from the covalent oxygen groups on graphene (Fig. 2d).

The morphologies of the $Ni(OH)_2$/graphene composites were investigated by scanning electron microscopy (SEM). Fig. 3a and b show representative SEM images of $Ni(OH)_2$/graphene, revealing a highly porous architecture, which is composed of nanoflakes with a thickness of 20–30 nm. No collapse of the Ni foam struts or obstruction of the pores is observed, indicating the strong mechanical strength of the $Ni(OH)_2$/graphene and the uniform dispersion of the $Ni(OH)_2$ nanosheets. Furthermore, the elemental mappings of C, O and Ni were investigated from a small region on the foam (Fig. 3c–f), indicating a continuous, uniform distribution of $Ni(OH)_2$ and graphene on the 3D Ni

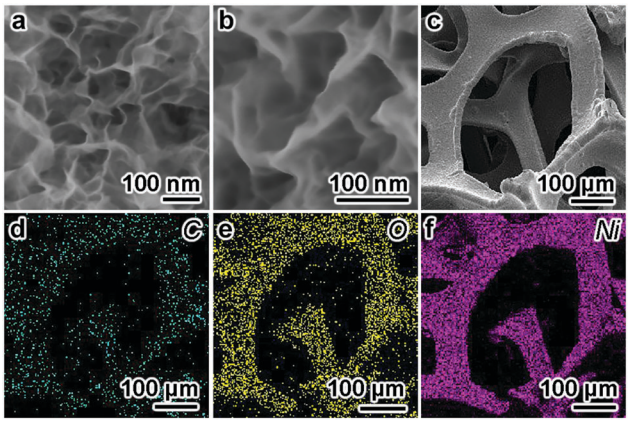

Fig. 3 Morphology and composition of the $Ni(OH)_2$/graphene composites. (a and b) SEM images of the $Ni(OH)_2$/graphene composite materials; (c) SEM image and the corresponding EDS elemental mapping images of (d) carbon, (e) oxygen, and (f) nickel.

foam surfaces. The corresponding EDS mapping also revealed that the C element content of the $Ni(OH)_2$/graphene composites is about 8% (atomic ratio, Table S1 in the ESI†), whereas there was no C element in the pristine $Ni(OH)_2$ without graphene on their surfaces (Fig. S4, ESI†). Fig. S5 (ESI†) shows that the sheet morphology of graphene and $Ni(OH)_2$ (black arrow markings), and a corresponding selected-area electron-diffraction pattern only indicate the typical sixfold symmetry expected for graphene. This result indicates an amorphous morphology of $Ni(OH)_2$. In addition, except for the peaks associated with the Ni foam substrate, no peaks are present in the X-ray diffraction pattern of $Ni(OH)_2$/graphene in Fig. S6 (ESI†), which further confirms the amorphous nature of the sample.

Further, we evaluated the electrochemical performance of the as-prepared $Ni(OH)_2$/graphene composites in a three-electrode test cell. The capacitive behavior of the electrode material is generally characterized using cyclic voltammetry (CV) curves. Fig. 4a presents typical CV curves of the $Ni(OH)_2$/graphene samples in a 1 M KOH electrolyte at various scan rates between 0.0 and 0.5 V. Two strong redox peaks can be observed in each curve. For electric double-layer capacitors, CV curves appear nearly rectangular. Our results thus indicate that the capacitance characteristics are mainly due to Faradaic redox reactions. For the $Ni(OH)_2$ electrode materials, the surface Faradaic reactions will proceed as:

$$Ni(OH)_2 + OH^- \leftrightarrow NiOOH + H_2O + e^-$$

To further evaluate the electrochemical properties and estimate the stable potential windows of the as-prepared $Ni(OH)_2$/graphene composites, galvanostatic charging and discharging of the films in 1 M KOH solution were performed using a Pt counter electrode and a saturated calomel reference electrode. The charge–discharge curves (Fig. 4b) at different current densities (2–16 mA cm^{-2}) between 0.0 and 0.6 V display slight nonlinearities that are very distinct from those of typical pure double-layer capacitors. This result indicates the occurrence of Faradaic reactions in the $Ni(OH)_2$/graphene composites.

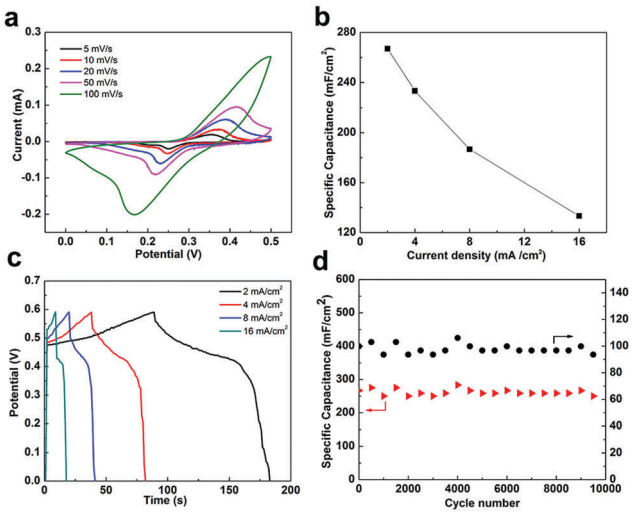

Fig. 4 Three-electrode electrochemical measurements of the $Ni(OH)_2$/graphene composites in 1 M KOH aqueous solution. (a) CV curves at different scan rates; (b) gravimetric specific capacitance of $Ni(OH)_2$/graphene composite as a function of the current densities; (c) galvanostatic charge discharge curves at various current densities; and (d) cycling performance of $Ni(OH)_2$/graphene composites at 2 mA cm^{-2}.

The specific capacitance of the $Ni(OH)_2$/graphene electrode can be calculated from the discharge curve according to $C = I \times \Delta t/(A \times \Delta V)$,[19] where I is the discharge current (A), Δt is the discharge time (s), A is the area of the active material in the electrode (cm^2) and ΔV is the potential change during discharge (V). The specific capacitances obtained were 267, 233, 187, and 133 mF cm^{-2} at current densities of 2, 4, 8 and 16 mA cm^{-2}, respectively. Clearly, the specific capacitance gradually decreases with increasing current density.

Good cycling stability is another important characteristic for high-performance supercapacitors. Fig. 4d reveals the cycle performance of the $Ni(OH)_2$/graphene samples measured at a current density of 2 mA cm^{-2} for 10 000 cycles. Afterward, the capacitance retention was 94.1% of the initial capacitance, indicating excellent long-term stability of the $Ni(OH)_2$/graphene composite electrode, which exceed those of the previously reported $Ni(OH)_2$-based materials (usually with a capacitance retention of 51.0–63.2% within 10 000 cycles).[15,20] By comparison, the 3D $Ni(OH)_2$ film without graphene presented a capacitance retention of only 41.4% even after 1000 cycles. These results highly highlight the vital role of the incorporation of graphene into electrochemical active electrode materials (Fig. S7, ESI†). Obviously, $Ni(OH)_2$/graphene has the smaller equivalent series resistance (ESR) value than $Ni(OH)_2$ as shown in Fig. S8 (ESI†), reflecting the enhancement in the electronic and ionic conductivities of $Ni(OH)_2$ with the presence of graphene. This result indicates that $Ni(OH)_2$/graphene composites exhibit good current rate properties, which are consistent with the cycle performance results.

In summary, we present a facile strategy to synchronously exfoliate graphite and assemble the high-quality graphene on 3D $Ni(OH)_2$ surfaces. High-quality graphene and the unique architecture of 3D skeleton provided $Ni(OH)_2$/graphene hybrids with high conductivity, strong mechanical stability, ion diffusivity as well as the capability to accommodate volume changes during Faradaic reactions. As a result, the resulting 3D $Ni(OH)_2$/graphene composites exhibited excellent specific capacitance, remarkable rate capability and super-long cycle life when used as electrode materials for supercapacitors. Such a simple and cost-effective synthetic approach would open new doors for the development of a serial of high-quality graphene based materials, and offer promising applications for high-performance energy-storage devices.

We acknowledge the support of the National 863 Program 2011AA050518 and the Natural Science Foundation of China (Grant no. 11174197, 11574203, and 61234005).

Notes and references

1 J. Zhang, J. Jiang, H. Li and X. S. Zhao, *Energy Environ. Sci.*, 2011, **4**, 4009–4015.
2 Z. Lei, J. Zhang and X. S. Zhao, *J. Mater. Chem.*, 2012, **22**, 153–160.
3 J.-W. Lang, L.-B. Kong, W.-J. Wu, Y.-C. Luo and L. Kang, *Chem. Commun.*, 2008, 4213–4215.

4 X.-H. Xia, J.-P. Tu, Y.-J. Mai, X.-L. Wang, C.-D. Gu and X.-B. Zhao, *J. Mater. Chem.*, 2011, **21**, 9319–9325.
5 S. K. Shinde, D. P. Dubal, G. S. Ghodake and V. J. Fulari, *RSC Adv.*, 2015, **5**, 4443–4447.
6 G. Wang, L. Zhang and J. Zhang, *Chem. Soc. Rev.*, 2012, **41**, 797–828.
7 (*a*) X. Xiong, D. Ding, D. Chen, G. Waller, Y. Bu, Z. Wang and M. Liu, *Nano Energy*, 2015, **11**, 154–161; (*b*) A. Harvey, X. He, I. J. Godwin, C. Backes, D. McAteer, N. C. Berner, N. McEvoy, A. Ferguson, A. Shmeliov, M. E. G. Lyons, V. Nicolosi, G. S. Duesberg, J. F. Donegan and J. N. Coleman, *J. Mater. Chem. A*, 2016, **4**, 11046–11059; (*c*) G.-W. Yang, C.-L. Xu and H.-L. Li, *Chem. Commun.*, 2008, 6537–6539; (*d*) Y. F. Yuan, X. H. Xia, J. B. Wu, J. L. Yang, Y. B. Chen and S. Y. Guo, *Electrochim. Acta*, 2011, **56**, 2627–2632.
8 Z. Tang, C. H. Tang and H. Gong, *Adv. Funct. Mater.*, 2012, **22**, 1272–1278.
9 Q. Huang, X. Wang, J. Li, C. Dai, S. Gamboa and P. J. Sebastian, *J. Power Sources*, 2007, **164**, 425–429.
10 (*a*) S. Yang, X. Wu, C. Chen, H. Dong, W. Hu and X. Wang, *Chem. Commun.*, 2012, **48**, 2773–2775; (*b*) J. Yan, Z. Fan, S. Wei, G. Ning, W. Tong, Z. Qiang, R. Zhang, L. Zhi and W. Fei, *Adv. Funct. Mater.*, 2012, **22**, 2632–2641; (*c*) S. Min, C. Zhao, G. Chen and X. Qian, *Electrochim. Acta*, 2014, **115**, 155–164; (*d*) C. H. Wu, S. X. Deng, H. Wang, Y. X. Sun, J. B. Liu and H. Yan, *ACS Appl. Mater. Interfaces*, 2014, **6**, 1106–1112.
11 (*a*) J. Yan, W. Sun, T. Wei, Q. Zhang, Z. Fan and F. Wei, *J. Mater. Chem.*, 2012, **22**, 11494–11502; (*b*) J. Xie, X. Sun, N. Zhang, K. Xu, M. Zhou and Y. Xie, *Nano Energy*, 2013, **2**, 65–74; (*c*) H. Wang, H. S. Casalongue, Y. Liang and H. Dai, *J. Am. Chem. Soc.*, 2010, **132**, 7472–7477; (*d*) C. Jiang, B. Zhan, C. Li, W. Huang and X. Dong, *RSC Adv.*, 2014, **4**, 18080–18085.
12 K. Parvez, Z.-S. Wu, R. Li, X. Liu, R. Graf, X. Feng and K. Müllen, *J. Am. Chem. Soc.*, 2014, **136**, 6083–6091.
13 W. Zhang, Y. Zeng, N. Xiao, H. H. Hng and Q. Yan, *J. Mater. Chem.*, 2012, **22**, 8455–8461.
14 M. Jing, C. Wang, H. Hou, Z. Wu, Y. Zhu, Y. Yang, X. Jia, Y. Zhang and X. Ji, *J. Power Sources*, 2015, **298**, 241–248.
15 L. Wang, X. Li, T. Guo, X. Yan and B. K. Tay, *Int. J. Hydrogen Energy*, 2014, **39**, 7876–7884.
16 C. Murli, S. M. Sharma, S. K. Kulshreshtha and S. K. Sikka, *Phys. Chem. Chem. Phys.*, 2001, **307**, 111–116.
17 M. C. Biesinger, L. W. M. Lau, A. R. Gerson and R. S. C. Smart, *Phys. Chem. Chem. Phys.*, 2012, **14**, 2434–2442.
18 H. B. Li, M. H. Yu, F. X. Wang, P. Liu, Y. Liang, J. Xiao, C. X. Wang, Y. X. Tong and G. W. Yang, *Nat. Commun.*, 2013, **4**(5), 54–56.
19 M. Jin, G. Zhang, F. Yu, W. Li, W. Lu and H. Huang, *Phys. Chem. Chem. Phys.*, 2013, **15**, 1601–1605.
20 J. Ji, L. L. Zhang, H. Ji, Y. Li, X. Zhao, X. Bai, X. Fan, F. Zhang and R. S. Ruoff, *ACS Nano*, 2013, **7**, 6237–6243.